Druitt, T.H., Kutterolf, S., Ronge, T.A., and the Expedition 398 Scientists
Proceedings of the International Ocean Discovery Program Volume 398
publications.iodp.org

Contents

Keywords
International Ocean Discovery Program, IODP, *JOIDES Resolution*, Expedition 398, Hellenic Arc Volcanic Field, Site U1589, Site U1590, Site U1591, Site U1593, Santorini, Kolumbo, pumice, submarine eruption, south Aegean volcanic arc, pumice raft, vesicularity, X-ray tomography

References (RIS)

MS 398-207
Received 7 February 2026
Accepted 8 June 2026
Published 31 August 2026

Data report: porosity and sinking times of pumice clasts from IODP Expedition 398, south Aegean volcanic arc[1]

Isabelle Susman,[2] Michael Manga,[2] Carla Escogido,[2] Tyler J. Cadena,[2] Sarah D. Ward,[3] Liam J. Kelly,[3] Kristen E. Fauria,[3] and the Expedition 398 Scientists[4]

[1] Susman, I., Manga, M., Escogido, C., Cadena, T.J., Ward, S.D., Kelly, L.J., Fauria, K.E., and the Expedition 398 Scientists, 2026. Data report: porosity and sinking times of pumice clasts from IODP Expedition 398, south Aegean volcanic arc. In Druitt, T.H., Kutterolf, S., Ronge, T.A., and the Expedition 398 Scientists, Hellenic Arc Volcanic Field. Proceedings of the International Ocean Discovery Program, 398: College Station, TX (International Ocean Discovery Program). https://doi.org/10.14379/iodp.proc.398.207.2026
[2] Department of Earth and Planetary Science, University of California, Berkley, USA. Correspondence author: **mmanga@berkeley.edu**
[3] Department of Earth and Environmental Sciences, Vanderbilt University, USA.
[4] **Expedition 398 Scientists' affiliations.**

Abstract

The porosities and sinking times of pumice clasts that interact with water determine whether they float and for how long they can be transported on the ocean surface before sinking. We report measurements for pumice clasts collected in cores recovered from five different drill sites and four different eruptions drilled during International Ocean Discovery Program (IODP) Expedition 398 on the south Aegean volcanic arc. Three eruptions were submarine (Archaeos, Kameni 726 Common Era [CE], and Kolumbo 1650 CE), and one eruption was a caldera-forming eruption from the Santorini complex (Lower Pumice 2). For each of 195 pumice clasts studied, we report total porosity and isolated porosity. We also report sinking times for the same set of pumice clasts on water for pumice at both room temperature and heated to 500°C before being dropped in water.

1. Introduction

The porosity of volcanic clasts provides a record of the processes of bubble nucleation, growth that accompanies decompression, coalescence, gas escape when the magma becomes permeable, and fragmentation. For these reasons, measurements of the porosity and texture of vesicles, such as their size distribution and shape, can be used to provide a window into ascent, eruption, and transport processes. During submarine eruptions, the thermal and physical properties of water lead to different ascent, fragmentation, and transport processes compared with subaerial eruptions (White et al., 2003; Cas and Simmons, 2018), and these processes may be recorded by volcanic clasts (Carey et al., 2018). For example, in submarine eruptions, the position of clasts within the submarine eruption column can affect the degree of seawater interaction, which impacts vesiculation, fragmentation, and hence vesicle connectivity, leading to lower connectivity in clasts at the edge of the column due to rapid quenching (Ward et al., 2025). Pumice porosity and textures from subaerial and submarine eruptions have overlapping characteristics (e.g., Cas and Giordano, 2014). In some cases, however, features such as a bimodal density spectrum have been attributed to quenching in water (Barker et al., 2012; Rotella et al., 2013). Submarine pumice may also contain a larger proportion of isolated vesicles from rapid quenching in water, even for high-vesicularity clasts (Ward et al., 2025).

For submarine eruptions and subaerial eruptions that deposit pumice clasts on the ocean surface from falls or density currents, the total and isolated porosity of volcanic clasts and the topology of pore spaces will determine whether the clasts will float on the ocean surface. The time clasts float can vary with clast porosity and size (Whitham and Sparks, 1986; Manville et al., 1998; White et al., 2001; Fauria et al., 2017) and their temperature when they interact with water (Whitham and Sparks, 1986; Dufek et al., 2007; Allen et al., 2008; Jutzeler et al., 2017; Fauria and Manga, 2018). If there are sufficient isolated vesicles relative to the total porosity, pumice clasts can also be unsinkable (Manga et al., 2018; Mitchell et al., 2021; Takeuchi et al., 2024; Yeo et al., 2024; Ward et al., 2025). Long flotation times enable long-distance transport in rafts of floating pumice (e.g., Richards, 1958; Bryan et al., 2012; Jutzeler et al., 2014; Fauria et al., 2023; Nagao et al., 2025). More generally, isolated porosity provides a window into ascent (Colombier et al., 2017, 2021; Mitchell et al., 2019), fragmentation (Nakamura et al., 2008; Mueller et al., 2011), and transport processes (Formenti and Druitt, 2003).

International Ocean Discovery Program (IODP) Expedition 398 to the south Aegean volcanic arc provided samples from explosive subaerial and submarine eruptions. One of the objectives of the expedition was to better understand the dynamics of submarine eruptions (**Druitt et al.**, 2024a). Here, we report measurements of total and connected porosity for 195 lapilli-sized pumice clasts from four different eruptions recovered from five sites cored during Expedition 398. We also report sinking times (how long they float) of the same clasts for cold (room temperature) and hot (500°C) pumice in room temperature water. These data may be useful in future studies of the transport and dispersal of volcanic clasts (e.g., Jutzeler et al., 2020; Nishikawa et al., 2023; Ishimura and Hiramine, 2025) for comparing and contrasting subaerial and submarine clasts (e.g., Ward et al., 2025) and provide clast-scale properties to help interpret seismic velocity measurements and bulk physical property measurements (e.g., Manga et al., 2025).

2. Samples and methods

Samples were recovered from the working halves of cores from seven holes at five sites for four different volcanic deposits. Three of the eruptions were submarine: Archaeos, Kameni 726 Common Era (CE), and Kolumbo 1650 CE. The fourth eruption, Lower Pumice 2, was subaerial. The Archaeos tuff was deposited by density currents produced by a ~765 ka (Metcalfe et al., 2025) shallow (<1 km) submarine rhyolite eruption with a volume >89 km^3 (Druitt et al., 2024b). Kameni 726 CE is the product of a postcaldera eruption within the Santorini Caldera formed by the 3.6 ka Minoan eruption. The pumice from this submarine eruption is part of a >3.6 km^3 deposit of tephra (Preine et al., 2024). Rhyolitic pumice from Kolumbo 1650 CE erupted from a submarine vent, with a maximum depth of 500 meters below sea level (mbsl) in the present 2 km^3 crater. (Cantner et al., 2014). Lower Pumice 2 is from a 177 ka caldera-forming rhyodacite eruption from the Santorini caldera complex (Wulf et al., 2020). Table **T1** summarizes the sampling depths, locations, and eruption ages. Drill site and sampled eruption locations are shown on the map in Figure **F1**.

Between 20 and 36 lapilli-sized pumice clasts were individually extracted from the working half of split cores. Clasts were handpicked using tweezers following core splitting to avoid clasts that were damaged during coring and subsequent splitting. Selected clasts were chosen to be representative of the sampled deposit. The number of clasts was less than the ideal number of >100 for measuring the porosity distribution (Shea et al., 2010) owing to the finite size of the recovered core and the need to preserve samples for other measurements. Each clast was assigned a unique identifier.

2.1. Total porosity

Samples were rinsed in tap water to remove surficial salts and then immersed in tap water and put under vacuum for 24 h to remove salt from the pore space. Clasts were then dried in an oven at 100°C for 24 h and weighed to obtain dry mass (M_c).

Archimedes' method was used to determine clast specific gravity by measuring clast weight in air and water following Houghton and Wilson (1989). Clasts were wrapped in a thin parafilm wax sheet to seal them from water infiltration and weighed to obtain the mass of parafilm on each clast

Table T1. Eruption characteristics of pumice samples, Expedition 398. **Download table in CSV format.**

(M_s). Clasts were then submerged in water, and because all clasts floated, their effective negative weight was determined (M_{c+s} water).

Specific gravity (SG) was calculated using

$$\mathrm{SG} = M_c\ \mathrm{air}/(M_c\ \mathrm{air} + M_s\ \mathrm{water} - M_{c+s}\ \mathrm{water}). \tag{1}$$

Bulk density (ρ_{bulk}) was calculated by multiplying SG by the density of water (ρ_w = 1 g/cm^3).

Clast envelope volume (V_E) was then calculated by dividing the clasts dry mass (M_c) by specific gravity:

$$V_E = \mathrm{SG}/M_c. \tag{2}$$

Total porosity (ϕ) was calculated as follows:

$$\phi = 1 - \mathrm{DRE/SG}. \tag{3}$$

We computed a dense rock equivalent (DRE) for the solid component of the clasts using measured and published compositions and the silicate melt density model of Iacovino and Till (2019), with an assumed 0.2 wt% H_2O in the glass. For the Archaeos and Kameni samples, we obtained a DRE of 2.40 and 2.53 g/cm^3 using the compositions reported in Druitt et al. (2024b) and Preine et al. (2024), respectively. For the Kolumbo samples, we used the composition of white rhyodacite from Druitt (2014) to obtain a density of 2.49 g/cm^3. For the Lower Pumice 2 samples, we used the composition of Unit B2 in Gertisser et al. (2009) to obtain a density of 2.50 g/cm^3.

2.2. Isolated porosity and connectivity

The skeletal volume (V_s) and density of each clast were determined using the AccuPyc II 1340 and 1345 gas pycnometers with helium as the working gas. For the analysis, the smallest sample cup that could accommodate the clast was selected to maximize accuracy because pycnometry is less reliable when the sample's volume is <10% of the cup's volume. The volume was calculated by introducing helium gas into the chamber with the sample and measuring the gas displaced. Each sample's volume and density were measured 10 times, and the average and standard deviation are reported.

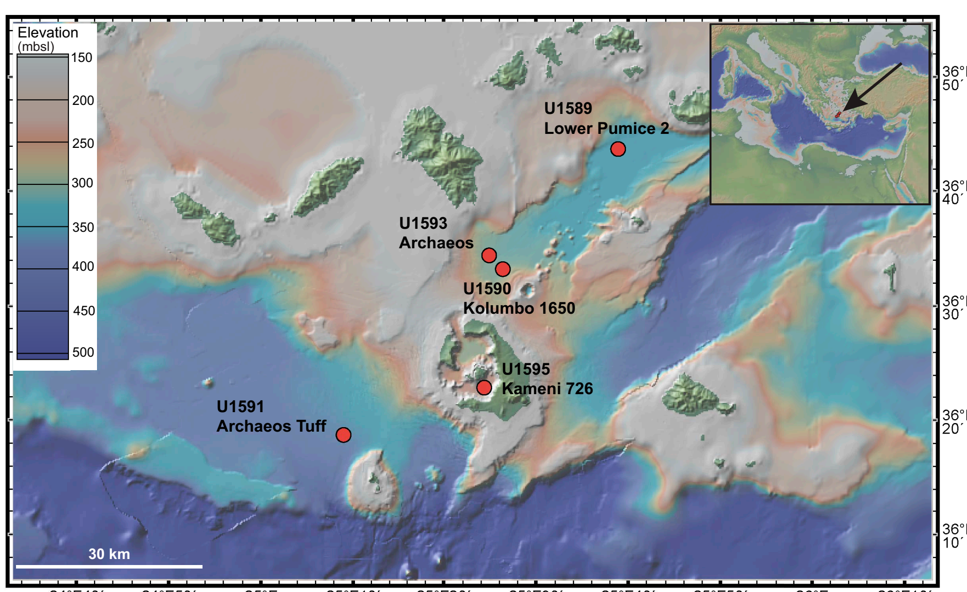

Figure F1. Regional map of central section of south Aegean volcanic arc, Expedition 398. Red dots = Expedition 398 drill sites from which samples were collected, green = areas above sea level. Inset: position of study area relative to Eastern Mediterranean. Figure made with GeoMapApp (**https://www.geomapapp.org**) CC BY Ryan et al. (2009).

Connected porosity (ϕ_C) was calculated from the skeletal volume (V_s) and envelope volume (V_E):

$$\phi_C = 1 - V_s/V_E. \quad (4)$$

Clast connectivity (C) is defined as

$$C = \phi_C/\phi. \quad (5)$$

Isolated porosity (ϕ_I) is the difference between total and connected porosity:

$$\phi_I = \phi - \phi_C. \quad (6)$$

2.3. Sinking times

To obtain the cold sinking time (t_c), dry clasts were placed in labeled tubes filled with room temperature tap water and set up in front of GoPro11 cameras. We did not use seawater to ensure that the water density did not change over the course of the experiment if there was evaporation. Timelapses with a 60 s interval were recorded. After a month, near-daily pictures were taken in addition to daily observation to avoid errors due to missing footage, difficulty in recognizing sinking in the video, or malfunctions such as power outages that turned off lights. Any clasts that sank without being recorded or were unable to sink because they got stuck in the tube were dehydrated again, and the experiment was repeated.

Hot sinking time (t_h) was measured by heating clasts to 500°C for 30 min in a ceramic crucible before dropping each clast from the crucible into room temperature water. Slow motion recordings of each clast being dropped were used to measure the time it took to sink after hitting the surface of the water.

2.4. X-ray computed tomography

To visualize the isolated pores, we imaged two clasts from the Kameni 726 CE eruption with X-ray computed microtomography (XRT) at the Advanced Light Source, Lawrence Berkeley National Laboratory. Samples were obtained from Section 398-U1595A-4H-3. These small pumice clasts, roughly 2–3 mm in diameter, were saturated under vacuum for 24 h and then soaked in water for 2 y to remove any gas from connected pore space. Imaging was performed with 28 keV monochromatic X-rays. Reconstructions used 1969 images collected over 180° of continuous rotation and an exposure time of 200 ms for each image. A 10× lens provided 0.635 µm voxel linear dimensions. Center of rotation corrections and artifact and ring removal procedures were performed during image reconstruction, whereby raw data was converted into stacks of tiff images. Preprocessing, including image smoothing and normalization, image segmentation, and 3D visualization were achieved with Dragonfly 3D World. Multiphase image segmentation of subvolumes (~0.25 mm × ~0.25 mm × ~0.25 mm cubes) of the clasts was performed with Dragonfly Segmentation Wizard. A subregion of one image slice in the chosen subvolume was hand-painted using the region of interest (ROI) tools to tag pixels corresponding to three classes: solids, water, and gas. This provided a training frame for a U-Net 3D convolutional neural network image segmentation model. The initial guess of the model was then applied to the entire image, and ROI tools were used to correct the model output. This process was repeated for several frames throughout the subvolume, and then all tagged frames were used for training and validation of the final U-Net model. This segmentation model was applied to the entire cubic subvolume, producing a 3D multiROI composed of solids, water, and gas. The volume of each phase was measured before converting the segmented data to a 3D rendering, where smoothing and coloring were applied for optimal visualization.

3. Results

Here, we report clast total porosities, isolated porosities, and sinking times. All data are tabulated in Table **T2**. Several clasts fractured upon entering water during the hot sinking experiments, and these are indicated with an "F" in the table.

Figure **F2** shows the total porosity for clasts from each of the four sampled eruptions. Total porosity of individual clasts ranges 0.57–0.91. The mean total porosity of the Archaeos samples (0.738 ± 0.059) is similar to the mean of 0.776 ± 0.044 for 18 clasts reported in Druitt et al. (2024b). The Lower Pumice 2 samples have the narrowest distribution of porosities and the highest mean total porosity (0.862 ± 0.016). The Kolumbo samples have a similar mean to Archaeos (0.765 ± 0.054). The Kameni samples have the second highest mean porosity at 0.835 ± 0.080. The mean isolated porosities in each deposit range from 0.022 (Lower Pumice 2) to 0.121 (Kolumbo 1650 CE). The isolated porosity for the Archaeos samples (0.054 ± 0.042) is slightly lower than the mean of 0.124 ± 0.038 for 18 clasts reported in Druitt et al. (2024b). If we used the solid density of 2.57 g/cm^3 adopted by Druitt et al. (2024b) in the calculation of total porosity (Equation **E3**) and isolated porosity (Equation **E6**), we recover similar means to Druitt et al. (2024b) for both total and isolated porosity (0.755 ± 0.055 and 0.071 ± 0.045, respectively).

Figure **F3** shows segmented 3D renderings of XRT images of subregions of two clasts from the Kameni 726 CE deposit. Both clasts have diameters of a few millimeters and are smaller than those on which we made porosity and sinking time measurements. The example shown in Figure **F3A** has properties similar to the larger Kameni clasts, with a total porosity of 0.85, similar to the mean of 0.84 for the 23 studied clasts. The isolated porosity in the imaged volume is smaller than the pycnometry data, and those isolated vesicles are preserved in the plateau borders between bubbles. The example shown in Figure **F3B** has a very different texture. The sample has a higher density with a total porosity of 0.17, and most of the vesicles are gas-filled with isolated porosity of 0.16. The texture of the vesicles, with elongated shapes terminating in cusps, is the product of strain to elongate the vesicles and collapse of those vesicles as the sample became permeable and

Table T2. Physical properties of pumice samples, Expedition 398. **Download table in CSV format.**

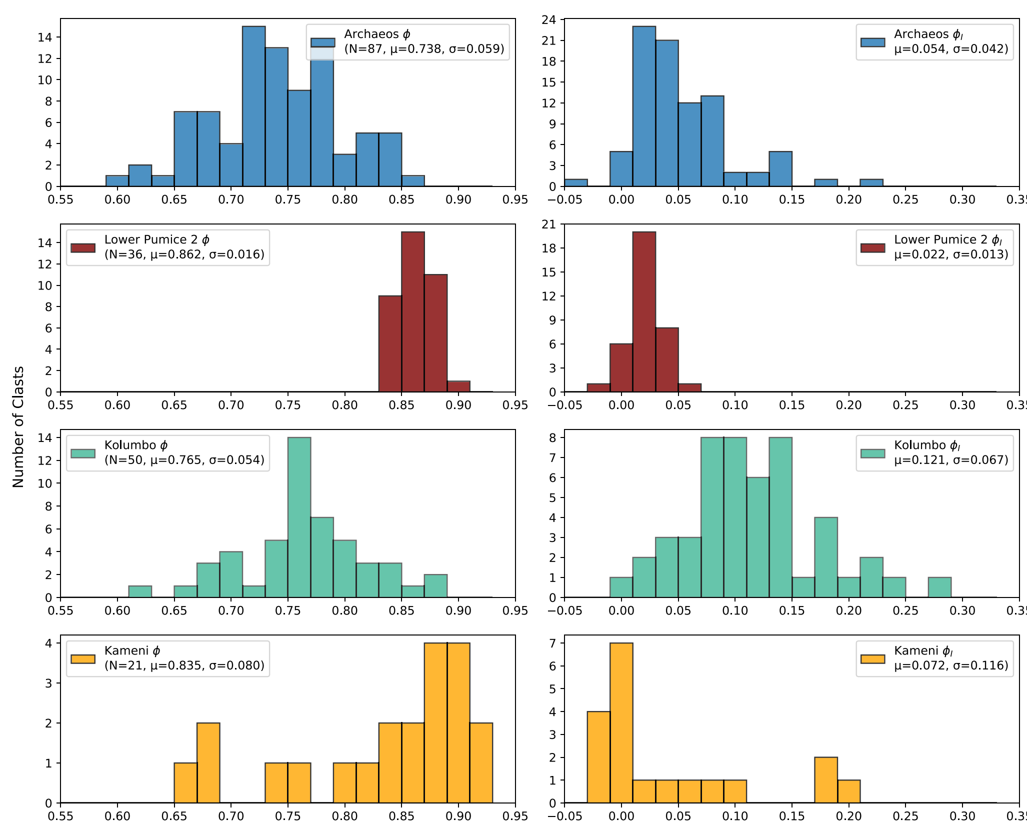

Figure F2. Histograms of total porosity (ϕ) and isolated porosity (ϕ_I) of clasts (expressed as fractions) from each eruption, Expedition 398. *N* = number of clasts, μ = mean values, σ = standard deviations.

gas escaped (e.g., Westrich and Eichelberger, 1994; Rust and Cashman, 2004). After the loss of gas and pore space collapse, the remaining vesicles are mostly isolated vesicles.

The pycnometry measurements in Figure **F2** and the example 3D rendering of segmented XRT images shown in Figure **F3** confirm that isolated vesicles can be preserved in the submarine settings we sampled. For the Archaeos samples, isolated porosity is preserved for 765 ka in present-day water depths >500 m and burial depths >135 m (Table **T1**); see also the isolated vesicles in XRT reconstructions of Archaeos samples presented in Manga et al. (2025). The strength of the quenched glass in the clasts must be sufficient to preserve pumice textures. Consequently, features of vesicles from tephra recovered from these cores can be used to study eruption processes.

Figure **F4** compares the connectivity and total porosity of our samples to those in the PePPEr database of porosity-connectivity measurements (**https://www.pepper-database.com**). Only samples identified as having a submarine source are shown in Figure **F4B**. All of our samples plot above the line that represents water-saturated clasts that have the density of seawater (ρ_w = 1.03 g/cm^3), given by

$$C = 1/\phi - (\mathrm{DRE}/\rho_w)\,(1/\phi - 1). \qquad (7)$$

We used two DRE densities for the solid fraction of 2.4 and 2.6 g/cm^3, a range that encompasses the values used here and those based on the highest values of bulk sediment measured for Archaeos (2.57 g/cm^3; Druitt et al., 2024b) and similar to Kameni (2.66 g/cm^3; Preine et al., 2024) samples. Bulk sediment DRE includes lithic fragments and hence may be higher than glass, although the use of glass for the DRE neglects the contributions from crystals that would increase the density. All of our samples are above the line, as expected for clasts that sank from fallout or were transported in gravity flows and were recovered from the seafloor.

Figure **F5** shows porosity, connectivity, cold sinking time, and hot sinking time against their clast envelope volumes for all eruptions. Uncertainties in porosity and connectivity increase as clast volume decreases.

We did not measure a strong trend of increasing sinking times with increasing clast size (R^2 = 0.23 for all hot pumice, R^2 = 0.02 for cold pumice), which contrasts with some previous studies (Whitham and Sparks, 1986; Manville et al., 1998; Fauria et al., 2017). Hot sinking time has a

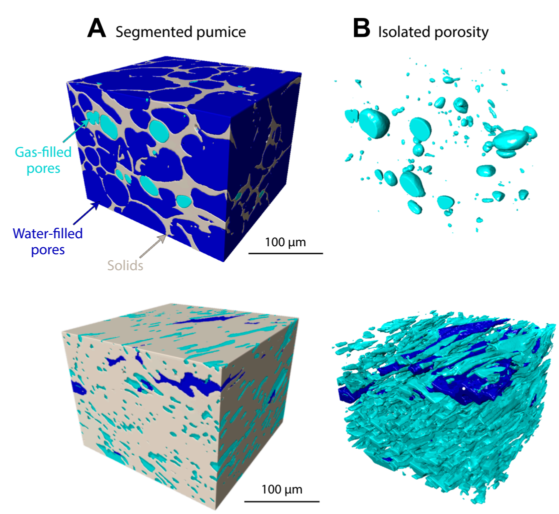

Figure F3. 3D renderings of XRT images of subvolumes of two clasts from the Kameni 726 CE eruption, Expedition 398. A. Segmented subvolume. Gray = solids (glass and any crystals), dark blue = water-filled (i.e., interconnected) vesicles, cyan = gas-filled (i.e., isolated) vesicles. B. Isolated vesicles (light blue) and a continuous curviplanar water-filled pore (dark blue) with solids removed from visualization. Low porosity sample in bottom row is not representative of bulk of pumice clasts, but it is shown to highlight textural diversity of clasts and geometry of connected and isolated pores in highly deformed samples that lost much of their porosity during deformation. Scale bars are approximate due to perspective. Images were collected on XRT beamline 8.3.2 of the Advanced Light Source using 28 keV monochromatic X-rays. Voxel linear dimension of tomography data is 0.635 µm.

stronger relationship with clast envelope volume compared with cold sinking time (Figure **F6**). Of all eruptions, clasts from Lower Pumice 2 had the strongest relationship between hot sinking time and clast envelope volume (R^2 = 0.25). Our measurements are consistent with Jutzeler et al. (2017), who found a correlation between clast volume and sinking time for hot pumice but not cold pumice.

We did not measure a relationship between connectivity and sinking time (R^2 = 0.04 for hot pumice, R^2 = 0.00 for cold pumice) (Figure **F7**). The majority of hot clasts sank in <7 s. This agrees with other hot sinking experiments where heating pumice clasts to temperatures above 400°C results in

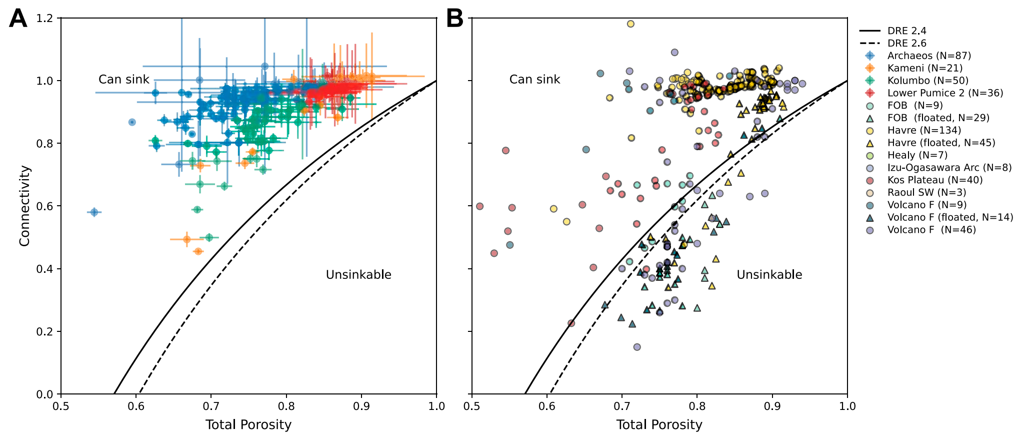

Figure F4. Total porosity of pumice samples versus their connectivity, Expedition 398. A. Sorted by eruption. To identify combinations of porosity and connectivity that make clasts unsinkable, we uses two different densities of the solid fraction of the clasts (DRE, 2.4 and 2.6 g/cm³) to encompass values reported for Archaeos and Kameni samples. Below these curves, pumice is prevented from sinking when connected porosity is filled with water because of sufficient isolated porosity. B. From PePPEr database (**https://www.pepper-database.com**). Triangles = samples collected from floating pumice rafts or washed onto shore, circles = samples collected on seafloor. Samples that plot above a connectivity of 1 are impossible and arise from (not always reported) uncertainty in measurements. FOB = Fukutoku-Oka-no-Ba.

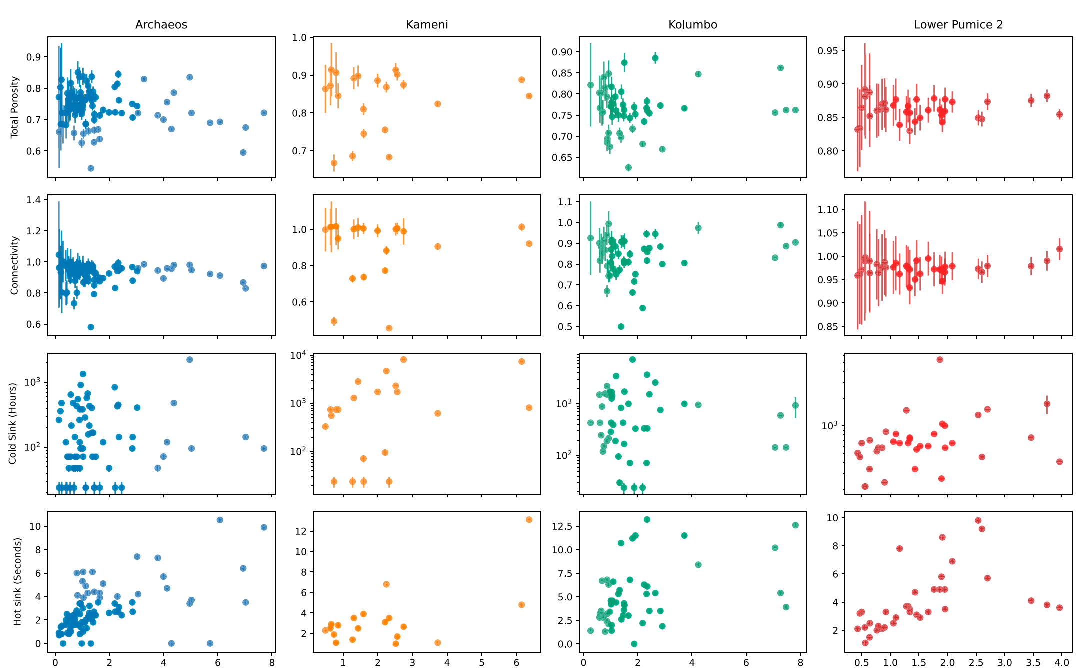

Figure F5. Porosity, connectivity, and cold and hot sinking time versus clast envelope volume for clasts from each eruption, Expedition 398. There is large scatter in sinking times across all eruptions. Cold sinking times are on log scale. One clast remained floating at time of submission (>675 days) and is not plotted. Clasts >8 cm³ (clast envelope volume) were too large for pycnometry and were excluded. Data points with no visible error bars have error bars smaller than symbol size.

efficient water ingestion as gas in connected pore space cools and contracts and water vapor condenses (Allen et al., 2008; Manga et al., 2018; Whitham and Sparks, 1986). Figure **F8** shows that there is no relationship between hot and cold sinking times.

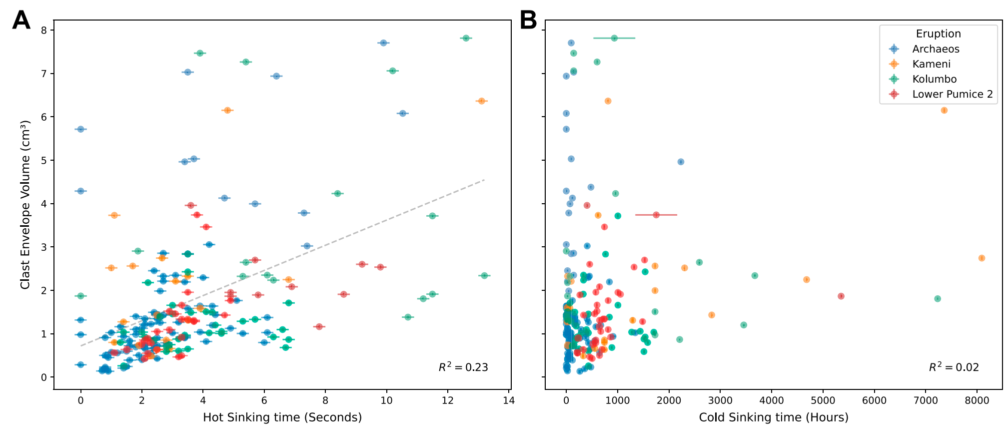

Figure F6. Clast envelope volume versus (A) hot sinking time and (B) cold sinking time, Expedition 398. Global R^2 values show stronger relationship for hot pumice than cold pumice. Linear regression line is shown for hot pumice (light gray dashed line) but not for cold pumice because R^2 is so small.

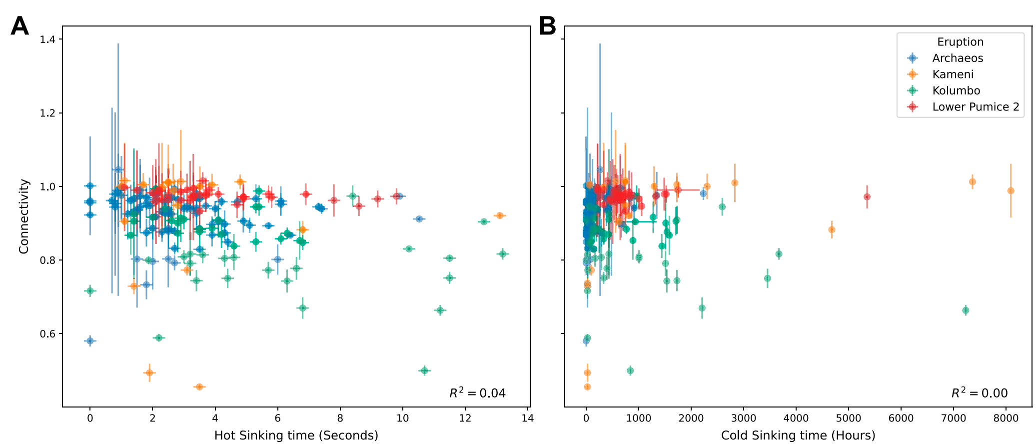

Figure F7. Relationship between clast connectivity and (A) hot sinking times and (B) cold sinking times, Expedition 398. Connectivity values >1 are impossible and due to measurement uncertainty.

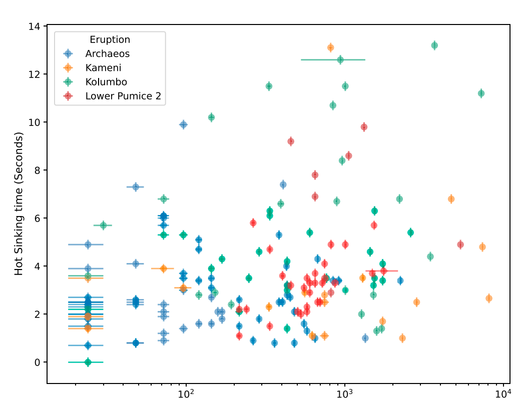

Figure F8. Relationship between hot sinking time and cold sinking time, Expedition 398. Cold sinking times are shown on log scale. Hot pumice clasts that fractured when entering water are not plotted.

4. Summary

We found that hot pumice clasts sink within seconds. Room temperature pumice clasts, however, float for much longer, typically weeks to >1 y. We did not find a strong correlation between clast volume and sinking times, with a weak correlation between clast volumes and hot sinking times and no relationship for cold sinking times. All samples of pumice from submarine eruptions contain isolated porosity, but the amount of isolated porosity is always insufficient to keep the recovered clasts from sinking when connected pores are filled with water. Interestingly, isolated porosity from the submarine Archaeos eruption is preserved in clasts >500 mbsl and >100 meters below seafloor (mbsf), as well as for 765 ka.

5. Acknowledgments

This research used samples provided by the International Ocean Discovery Program (IODP). We thank the crew, staff, and technicians on the research vessel (R/V) *JOIDES Resolution* during Expedition 398. M. Manga, I. Susman, and C. Escogido received support from the US Science Support Program (USSSP) postexpedition activity (PEA) grant and the Undergraduate Research Apprenticeship Program (URAP) at University of California, Berkeley. X-ray computed tomography was made possible with the support of the Department of Energy Advanced Light Source beamline 8.3.2 and beamline scientists Dula Parkinson and Elizabeth Clark. We thank M.O. Manga for watching pumice and recording sinking times and J. Grimsich for helping set up laboratory facilities. We thank Leah LeVay and Martin Jutzeler for thoughtful and careful reviews. Expedition 398 and the JOIDES Resolution Science Operator (JRSO) were funded by National Science Foundation (NSF) Award OCE 1326927.

References

Allen, S.R., Fiske, R.S., and Cashman, K.V., 2008. Quenching of steam-charged pumice: implications for submarine pyroclastic volcanism. Earth and Planetary Science Letters, 274(1):40–49. **https://doi.org/10.1016/j.epsl.2008.06.050**

Barker, S.J., Rotella, M.D., Wilson, C.J.N., Wright, I.C., and Wysoczanski, R.J., 2012. Contrasting pyroclast density spectra from subaerial and submarine silicic eruptions in the Kermadec arc: implications for eruption processes and dredge sampling. Bulletin of Volcanology, 74(6):1425–1443. **https://doi.org/10.1007/s00445-012-0604-2**

Bryan, S.E., Cook, A.G., Evans, J.P., Hebden, K., Hurrey, L., Colls, P., Jell, J.S., Weatherley, D., and Firn, J., 2012. Rapid, long-distance dispersal by pumice rafting. PloS One, 7(7):e40583. **https://doi.org/10.1371/journal.pone.0040583**

Cantner, K., Carey, S., and Nomikou, P., 2014. Integrated volcanologic and petrologic analysis of the 1650AD eruption of Kolumbo submarine volcano, Greece. Journal of Volcanology and Geothermal Research, 269:28–43. **https://doi.org/10.1016/j.jvolgeores.2013.10.004**

Carey, R., Soule, S.A., Manga, M., White, J.D.L., McPhie, J., Wysoczanski, R., Jutzeler, M., Tani, K., Yoerger, D., Fornari, D., Caratori-Tontini, F., Houghton, B., Mitchell, S., Ikegami, F., Conway, C., Murch, A., Fauria, K., Jones, M., Cahalan, R., and McKenzie, W., 2018. The largest deep-ocean silicic volcanic eruption of the past century. Science Advances, 4(1):e1701121. **https://doi.org/10.1126/sciadv.1701121**

Cas, R.A.F., and Giordano, G., 2014. Submarine volcanism: a review of the constraints, processes and products, and relevance to the Cabo de Gata volcanic succession. Italian Journal of Geosciences, 133(3):362–377. **https://doi.org/10.3301/IJG.2014.46**

Cas, R.A.F., and Simmons, J.M., 2018. Why deep-water eruptions are so different from subaerial eruptions. Frontiers in Earth Science, 6:198. **https://doi.org/10.3389/feart.2018.00198**

Colombier, M., Vasseur, J., Houghton, B.F., Cáceres, F., Scheu, B., Kueppers, U., Thivet, S., Gurioli, L., Montanaro, C., Soldati, A., Di Muro, A., and Dingwell, D.B., 2021. Degassing and gas percolation in basaltic magmas. Earth and Planetary Science Letters, 573:117134. **https://doi.org/10.1016/j.epsl.2021.117134**

Colombier, M., Wadsworth, F.B., Gurioli, L., Scheu, B., Kueppers, U., Di Muro, A., and Dingwell, D.B., 2017. The evolution of pore connectivity in volcanic rocks. Earth and Planetary Science Letters, 462:99–109. **https://doi.org/10.1016/j.epsl.2017.01.011**

Druitt, T.H., 2014. New insights into the initiation and venting of the Bronze-Age eruption of Santorini (Greece), from component analysis. Bulletin of Volcanology, 76(2):794. **https://doi.org/10.1007/s00445-014-0794-x**

Druitt, T.H., Kutterolf, S., Ronge, T.A., Beethe, S., Bernard, A., Berthod, C., Chen, H., Chiyonobu, S., Clark, A., DeBari, S., Fernandez Perez, T.I., Gertisser, R., Hübscher, C., Johnston, R.M., Jones, C., Joshi, K.B., Kletetschka, G., Koukousioura, O., Li, X., Manga, M., McCanta, M., McIntosh, I., Morris, A., Nomikou, P., Pank, K., Peccia, A., Polymenakou, P.N., Preine, J., Tominaga, M., Woodhouse, A., and Yamamoto, Y., 2024a. Expedition 398 summary. In Druitt, T.H., Kutterolf, S., Ronge, T.A., and the Expedition 398 Scientists, Hellenic Arc Volcanic Field. Proceedings of the International Ocean Discovery Program, 398: College Station, TX (International Ocean Discovery Program). **https://doi.org/10.14379/iodp.proc.398.101.2024**

Druitt, T.H., Kutterolf, S., Ronge, T.A., Hübscher, C., Nomikou, P., Preine, J., Gertisser, R., Karstens, J., Keller, J., Koukousioura, O., Manga, M., Metcalfe, A., McCanta, M., McIntosh, I., Pank, K., Woodhouse, A., Beethe, S., Berthod, C., Chiyonobu, S., Chen, H., Clark, A., DeBari, S., Johnston, R., Peccia, A., Yamamoto, Y., Bernard, A., Perez, T.F., Jones, C., Joshi, K.B., Kletetschka, G., Li, X., Morris, A., Polymenakou, P., Tominaga, M., Papanikolaou, D., Wang, K.-L., and Lee, H.-Y., 2024b. Giant offshore pumice deposit records a shallow submarine explosive eruption of ancestral Santorini. Communications Earth & Environment, 5(1). **https://doi.org/10.1038/s43247-023-01171-z**

Dufek, J., Manga, M., and Staedter, M., 2007. Littoral blasts: pumice-water heat transfer and the conditions for steam explosions when pyroclastic flows enter the ocean. Journal of Geophysical Research: Solid Earth, 112(B11). **https://doi.org/10.1029/2006JB004910**

Fauria, K.E., Jutzeler, M., Mittal, T., Gupta, A.K., Kelly, L.J., Rausch, J., Bennartz, R., Delbridge, B., and Retailleau, L., 2023. Simultaneous creation of a large vapor plume and pumice raft by the 2021 Fukutoku-Oka-no-Ba shallow submarine eruption. Earth and Planetary Science Letters, 609:118076. **https://doi.org/10.1016/j.epsl.2023.118076**

Fauria, K.E., and Manga, M., 2018. Pyroclast cooling and saturation in water. Journal of Volcanology and Geothermal Research, 362:17–31. **https://doi.org/10.1016/j.jvolgeores.2018.07.002**

Fauria, K.E., Manga, M., and Wei, Z., 2017. Trapped bubbles keep pumice afloat and gas diffusion makes pumice sink. Earth and Planetary Science Letters, 460:50–59. **https://doi.org/10.1016/j.epsl.2016.11.055**

Formenti, Y., and Druitt, T.H., 2003. Vesicle connectivity in pyroclasts and implications for the fluidisation of fountain-collapse pyroclastic flows, Montserrat (West Indies). Earth and Planetary Science Letters, 214(3):561–574. **https://doi.org/10.1016/S0012-821X(03)00386-8**

Gertisser, R., Preece, K., and Keller, J., 2009. The Plinian Lower Pumice 2 eruption, Santorini, Greece: magma evolution and volatile behaviour. Journal of Volcanology and Geothermal Research, 186(3):387–406. **https://doi.org/10.1016/j.jvolgeores.2009.07.015**

Houghton, B.F., and Wilson, C.J.N., 1989. A vesicularity index for pyroclastic deposits. Bulletin of Volcanology, 51(6):451–462. **https://doi.org/10.1007/BF01078811**

Iacovino, K., and Till, C.B., 2019. DensityX: a program for calculating the densities of magmatic liquids up to 1,627 °C and 30 kbar. Volcanica, 2(1):1–10. **https://doi.org/10.30909/vol.02.01.0110**

Ishimura, D., and Hiramine, R., 2025. Dispersion, fragmentation, abrasion, and organism attachment of drift pumice from the 2021 Fukutoku-Oka-no-Ba eruption in Japan. Progress in Earth and Planetary Science, 12(1):5. **https://doi.org/10.1186/s40645-024-00678-z**

Jutzeler, M., Manga, M., White, J.D.L., Talling, P.J., Proussevitch, A.A., Watt, S.F.L., Cassidy, M., Taylor, R.N., Le Friant, A., and Ishizuka, O., 2017. Submarine deposits from pumiceous pyroclastic density currents traveling over water: an outstanding example from offshore Montserrat (IODP 340). Geological Society of America Bulletin, 129(3):392–414. **https://doi.org/10.1130/B31448.1**

Jutzeler, M., Marsh, R., Carey, R.J., White, J.D.L., Talling, P.J., and Karlstrom, L., 2014. On the fate of pumice rafts formed during the 2012 Havre submarine eruption. Nature Communications, 5(1):3660. **https://doi.org/10.1038/ncomms4660**

Jutzeler, M., Marsh, R., van Sebille, E., Mittal, T., Carey, R.J., Fauria, K.E., Manga, M., and McPhie, J., 2020. Ongoing dispersal of the 7 August 2019 pumice raft from the Tonga arc in the southwestern Pacific Ocean. Geophysical Research Letters, 47(5):e1701121. **https://doi.org/10.1029/2019GL086768**

Manga, M., Fauria, K.E., Lin, C., Mitchell, S.J., Jones, M.P., Conway, C.E., Degruyter, W., Hosseini, B., Carey, R., Cahalan, R., Houghton, B.F., White, J.D.L., Jutzeler, M., Soule, S.A., and Tani, K., 2018. The pumice raft-forming 2012 Havre submarine eruption was effusive. Earth and Planetary Science Letters, 489:49–58. **https://doi.org/10.1016/j.epsl.2018.02.025**

Manga, M., Wright, V., Cadena, T., McIntosh, I., Preine, J., Tominaga, M., Nomikou, P., Druitt, T., Kutterolf, S., Beethe, S., Ronge, T.A., Hübscher, C., Karstens, J., Kletetschka, G., Yamamoto, Y., Woodhouse, A., Gertisser, R., Peccia, A., Clark, A., and IODP Expedition 398 Participants, 2025. Contrasting seismic velocity and compaction of marine calcareous oozes and volcaniclastic deposits on the South Aegean Volcanic Arc. Geochemistry, Geophysics, Geosystems, 26(9):e2025GC012327. **https://doi.org/10.1029/2025GC012327**

Manville, V., White, J.D.L., Houghton, B.F., and Wilson, C.J.N., 1998. The saturation behaviour of pumice and some sedimentological implications. Sedimentary Geology, 119(1):5–16. **https://doi.org/10.1016/S0037-0738(98)00057-8**

Metcalfe, A., Druitt, T., Pank, K., Kutterolf, S., Preine, J., Beethe, S., Schmitt, A., Hübscher, C., Nomikou, P., Ronge, T.A., Berthod, C., Chen, H., Chiyonobu, S., Clark, A., DeBari, S., Gertisser, R., Johnston, R., Koukousioura, O., Manga, M., McCanta, M., McIntosh, I., Peccia, A., Tominaga, M., Yamamoto, Y., Woodhouse, A., Bernard, A., Perez, T.F., Jones, C.K., Joshi, K.B., Kletetschka, G., Morris, A., Polymenakou, P., Li, X., Papanikolaou, D., Pyle, D., and Sternai, P., 2025. Tectonic modulation of caldera volcanism on the South Aegean Volcanic Arc. Earth and Planetary Science Letters, 671:119633. **https://doi.org/10.1016/j.epsl.2025.119633**

Mitchell, S.J., Fauria, K.E., Houghton, B.F., and Carey, R.J., 2021. Sink or float: microtextural controls on the fate of pumice deposition during the 2012 submarine Havre eruption. Bulletin of Volcanology, 83(11):80. **https://doi.org/10.1007/s00445-021-01497-6**

Mitchell, S.J., Houghton, B.F., Carey, R.J., Manga, M., Fauria, K.E., Jones, M.P., Soule, S.A., Conway, C.E., Wei, Z., and Giachetti, T., 2019. Submarine giant pumice: a window into the shallow conduit dynamics of a recent silicic eruption. Bulletin of Volcanology, 81(7):42. **https://doi.org/10.1007/s00445-019-1298-5**

Mueller, S., Scheu, B., Kueppers, U., Spieler, O., Richard, D., and Dingwell, D.B., 2011. The porosity of pyroclasts as an indicator of volcanic explosivity. Journal of Volcanology and Geothermal Research, 203(3):168–174. **https://doi.org/10.1016/j.jvolgeores.2011.04.006**

Nagao, R., Yokoyama, T., and Takeuchi, S., 2025. Pumice flotation time: how does the infiltration of water progress inside pumice? Progress in Earth and Planetary Science, 12(1):82. **https://doi.org/10.1186/s40645-025-00750-2**

Nakamura, M., Otaki, K., and Takeuchi, S., 2008. Permeability and pore-connectivity variation of pumices from a single pyroclastic flow eruption: implications for partial fragmentation. Journal of Volcanology and Geothermal Research, 176(2):302–314. **https://doi.org/10.1016/j.jvolgeores.2008.04.011**

Nishikawa, H., Kuwatani, T., Tada, N., and Kayama Watanabe, H., 2023. Simulated distributions of pumice rafts in Japan following eruptions at volcanic islands and submarine volcanoes. Progress in Earth and Planetary Science, 10(1):21. **https://doi.org/10.1186/s40645-023-00552-4**

Preine, J., Karstens, J., Hübscher, C., Druitt, T., Kutterolf, S., Nomikou, P., Manga, M., Gertisser, R., Pank, K., Beethe, S., Berthod, C., Crutchley, G., McIntosh, I., Ronge, T., Tominaga, M., Clark, A., DeBari, S., Johnston, R., Mateo, Z., Peccia, A., Jones, C., Kletetschka, G., Metcalfe, A., Bernard, A., Chen, H., Chiyonobu, S., Fernandez-Perez, T., Joshi, K.B., Koukousioura, O., McCanta, M., Morris, A., Polymenakou, P., Woodhouse, A., Yamamoto, Y., Wang, K.-L., Lee, H.-Y., Li, X., and Papanikolaou, D., 2024. Hazardous explosive eruptions of a recharging multi-cyclic island arc caldera. Nature Geoscience, 17:323–331. **https://doi.org/10.1038/s41561-024-01392-7**

Richards, A.F., 1958. Transpacific distribution of floating pumice from Isla San Benedicto, Mexico. Deep Sea Research (1953), 5(1):29–35. **https://doi.org/10.1016/S0146-6291(58)80005-3**

Rotella, M.D., Wilson, C.J.N., Barker, S.J., and Wright, I.C., 2013. Highly vesicular pumice generated by buoyant detachment of magma in subaqueous volcanism. Nature Geoscience, 6(2):129–132. **https://doi.org/10.1038/ngeo1709**

Rust, A.C., and Cashman, K.V., 2004. Permeability of vesicular silicic magma: inertial and hysteresis effects. Earth and Planetary Science Letters, 228(1):93–107. **https://doi.org/10.1016/j.epsl.2004.09.025**

Ryan, W.B.F., Carbotte, S.M., Coplan, J.O., O'Hara, S., Melkonian, A., Arko, R., Weissel, R.A., Ferrini, V., Goodwillie, A., Nitsche, F., Bonczkowski, J., and Zemsky, R., 2009. Global multi-resolution topography synthesis. Geochemistry, Geophysics, Geosystems, 10(3):Q03014. **https://doi.org/10.1029/2008GC002332**

Shea, T., Houghton, B.F., Gurioli, L., Cashman, K.V., Hammer, J.E., and Hobden, B.J., 2010. Textural studies of vesicles in volcanic rocks: an integrated methodology. Journal of Volcanology and Geothermal Research, 190(3):271–289. **https://doi.org/10.1016/j.jvolgeores.2009.12.003**

Takeuchi, S., Ishige, K., Uesawa, S., and Suwa, Y., 2024. Unsinkable, long-drifting, millimeter-sized pumice of the 2021 eruption of Fukutoku-Oka-no-Ba submarine volcano. Progress in Earth and Planetary Science, 11(1):47. **https://doi.org/10.1186/s40645-024-00652-9**

Ward, S.D., Fauria, K.E., Jutzeler, M., Dasent, J., and Wright, V., 2025. Isolated vesicles in submarine pumice: insights from the 2019 Volcano F eruption, Kingdom of Tonga. Bulletin of Volcanology, 87(12):114. **https://doi.org/10.1007/s00445-025-01905-1**

Westrich, H.R., and Eichelberger, J.C., 1994. Gas transport and bubble collapse in rhyolitic magma: an experimental approach. Bulletin of Volcanology, 56(6):447–458. **https://doi.org/10.1007/BF00302826**

White, J.D.L., Manville, V., Wilson, C.J.N., Houghton, B.F., Riggs, N.R., and Ort, M., 2001. Settling and deposition of AD 181 Taupo pumice in lacustrine and associated environments. In White, J.D.L. and Riggs, N.R., Volcaniclastic Sedimentation in Lacustrine Settings. 141–150. **https://doi.org/10.1002/9781444304251.ch7**

White, J.D.L., Smellie, J.L., and Clague, D.A., 2003. Introduction: a deductive outline and topical overview of subaqueous explosive volcanism. In White, J.D.L., Smellie, J.L. and Clague, D.A., Explosive Subaqueous Volcanism. 1–23. **https://doi.org/10.1029/140GM01**

Whitham, A.G., and Sparks, R.S.J., 1986. Pumice. Bulletin of Volcanology, 48(4):209–223. **https://doi.org/10.1007/BF01087675**

Wulf, S., Keller, J., Satow, C., Gertisser, R., Kraml, M., Grant, K.M., Appelt, O., Vakhrameeva, P., Koutsodendris, A., Hardiman, M., Schulz, H., and Pross, J., 2020. Advancing Santorini's tephrostratigraphy: new glass geochemical data and improved marine-terrestrial tephra correlations for the past ~360 kyrs. Earth-Science Reviews, 200:102964. **https://doi.org/10.1016/j.earscirev.2019.102964**

Yeo, I.A., McIntosh, I.M., Bryan, S.E., Tani, K., Dunbabin, M., Dobson, K.J., Mitchell, S.J., Collins, P.C., Clare, M.A., Cathey, H., Duwai, I., Brandl, P.A., Stone, K., and Manu, M.S., 2024. The 2019 pumice raft forming eruption of Volcano-F (Volcano 0403–091) and implications for hazards posed by submerged calderas. Journal of Volcanology and Geothermal Research, 454:108160. **https://doi.org/10.1016/j.jvolgeores.2024.108160**